Int J Adv Manuf Technol (2013) 69:181–195
DOI 10.1007/s00170-013-5015-9

ORIGINAL ARTICLE

Effect of weld characteristics on the formability of welded tubes in NC bending process

Ning Ren · He Yang · Mei Zhan · Zhi-Yong Zhang · Hao-Min Jiang · Ke-Shan Diao · Xin-Ping Chen

Received: 2 July 2012 / Accepted: 16 April 2013 / Published online: 28 April 2013

Abstract The weld profiles, weld width, weld positions, and mechanical property changes in the weld and heat-affected zones (HAZ) are the most important parameters that influence the potential formability of the welded tube. To investigate the effect of weld characteristics on the forming behaviors of the welded tube, finite element models which consider the geometric profile and mechanical properties of the weld and HAZ are employed. The results show that (1) the mechanical constitutive relation of the weld region determined by the microhardness empirical formula obviously decreases the tangent strain, thickness strain, and cross-sectional deformation ΔD in the weld and HAZ as compared with that determined by the improved rule of mixtures, which is contrary to the hoop strain, and the predicted results determined by the improved rule of mixtures are much closer to the experimental ones; (2) different weld and HAZ widths determined by the microhardness profile and metallographic section have a little effect on the tangent strain, thickness strain, and ΔD distribution; (3) the implementation of weld profile and material properties decreases the wall variation of the weld region as the weld line locates on the outside and inside. On the contrary, both the weld profile and weld material properties increase the maximum ΔD. The sectorial weld profile has a stronger effect on the wall variation and maximum ΔD than the hourglass profile; and (4) the same weld and HAZ volume have a stronger effect on wall thinning and ΔD.

N. Ren (✉) · H. Yang · M. Zhan · Z.-Y. Zhang
State Key Laboratory of Solidification Processing, School of Materials Science and Engineering, Northwestern Polytechnical University, Xi'an 710072, People's Republic of China
e-mail: renning12@mail.nwpu.edu.cn

H.-M. Jiang · K.-S. Diao · X.-P. Chen
Baosteel Group Corporation, Shanghai 200122, People's Republic of China

Keywords Weld characteristics · Welded tube · NC bending · FE simulation · Rule of mixtures

1 Introduction

In the automotive industry, the application of tailor-welded blanks (TWBs) and welded tubes is becoming more widespread in recent years from the viewpoints of automobile weight reduction, improved collision safety, and cost reduction [1–3]. In many applications, the welded tubes require a bending operation for making a wide variety of structural components. Numerical control (NC) rotary draw bending is one of the most commonly used tube bending processes due to its advantages such as being an efficient, economical, and stable forming process and making easier to achieve the digital precision forming process [4]. The welded tube NC bending process is shown in Fig. 1.

Despite the numerous benefits, the welded tube NC bending is challenging due to the significant reduction of formability. The welded tube is generally divided into three different regions: the fusion zone, or weld metal, the heat-affected zone (HAZ), and the unaffected parent zone. Each of these zones possesses individual mechanical properties. The inherent characteristics of some welding processes such as high strength, high hardness, low ductility, and wide weld make the weld region be regions of stress concentration where fatigue cracks are likely to initiate. The non-uniform deformation induced by differences in material properties, thickness, and weld location will reduce the potential formability of the welded tube. Panda et al. [5] showed that the weld ductility and the extent of difference in properties were the most important parameters for formability in TWBs with differences in properties.

Different welding techniques may produce welds with different profiles and properties. Many researches have

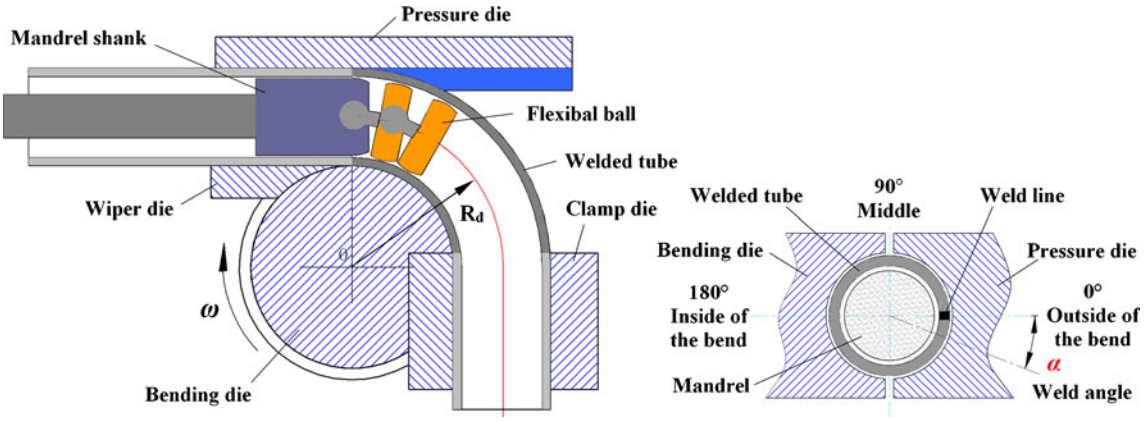

Fig. 1 Schematic diagrams of welded tube NC bending process and weld position

shown that there are obvious differences in the weld profile, microstructure, microhardness, and mechanical properties of the weld metal, HAZ material, and parent metal. Regardless of the frequency of the power source used to make longitudinal butt welds in tube and pipe, a discernible hourglass shape signature is present when the high-frequency electric resistance welding (HF-ERW) process is used. Kim et al. [6] concluded that the weld metal had larger strength coefficient, strain hardening exponent, and microhardness than the parent metal of the steel welded tube produced by HF-ERW. Bhagwan et al. [7] showed that the weld of the AA5182-O TWBs manufactured by the gas tungsten arc welding process had a crown shape with a smooth elevation in the middle section of its topside; the weld was about 4.6 mm in width, with a maximum height of about 1.96 mm in the middle of the profile, and the weld had lower strength coefficient and strain hardening exponent as compared with the parent metal. Panda et al. [8] reported that the weld specimens produced by laser welding was significantly higher in strength and lower in ductility compared with the surrounding material. The weld of ZK21 magnesium alloy sheet joined by laser welding had only slightly lower values in hardness than the parent metal [9]. The different material properties in the weld region make a notable distinction between the welded part and homogeneous tube and sheet deformation. Hamidinejad et al. [10] reported that the specimens showed a failure type initiating in the softened region located in the HAZ during Erichsen cupping test. In addition, the weld geometry has a significant effect on the forming quality of the weldment. Bhagwan et al. [7] modeled the weld region as a separate zone and calculated that weld profile was possibly more important than considering the mechanical properties of the weld zone during the TWB forming analysis, and the welding process used to join the blanks, the weld orientation, the weld geometry, and the mechanical properties of the weld could affect the deformation behavior of the weld region. Imaninejad et al. [11] showed that a semi-circular weld moved the failure location further away from the weld center compared to a rectangular weld, and the weld width had little effect on the maximum stress. Nguyen et al. [12] showed that the fatigue life and fatigue strength of the weld region were greatly affected by the geometry of the weld. However, in the published literature on numerical investigations of the formability of TWBs and welded tube, for modeling of the weld region, most of the analyses that have been carried out are based on simplified models that neglect either weld geometry or weld properties [13–15]. In some special cases, especially when the weld suffers a large deformation, ignoring the weld characteristic would cause a significant loss in accuracy [16]. So far, the effect of weld geometry parameters on the deformation behaviors in welded tube NC bending process is rarely determined. Therefore, modeling of the weld profile is essential for the finite element (FE) analysis of the welded tube NC bending. In three-dimensional solid finite element models, the weld geometry profile can be exactly described based on the etched metallographic section of the weld region.

Knowledge of the mechanical properties of the weld is critical to develop a numerical model that can accurately predict the forming behaviors of the weld region. Generally speaking, since the different regions of the welded tube should be individually modeled in the simulation, the mechanical properties of weld metal and HAZ material must be provided quantitatively for the simulation. Several techniques have been employed to determine the mechanical properties of the weld region, which mainly include the subsize specimen tensile test [17], empirical formula based on microhardness test [18], and rule of mixtures [19]. Recently, the rule of mixture had become a commonly used method for estimating the mechanical properties of the weld region [20–22]. To obtain a more precise mechanical property of a welded tube with an extremely narrow weld that cannot cut into specimens, an improved rule of mixtures [23] is adopted in this paper. Meanwhile, the mechanical properties of the weld

region determined by the microhardness empirical formula are achieved for comparison.

Waddell et al. [24] found that the formability of the TWBs produced by laser welding was related to weld hardness and weld width. The accurate measurement of weld width is necessary to demonstrate the forming features of the weld region. There are a number of methods by which the width can be determined, including direct measurement of weld width by visual inspection, estimation of weld width from a metallographic section, and microhardness profiles. Kim et al. [6] determined the width of the weld and HAZ through the microhardness profile according to the principle that the microhardness across the weld metal and HAZ was different from the parent metal. Kridli et al. [25] obtained the weld width through metallographic analysis according to the principle that the microstructure across the weld metal and HAZ was different from the parent metal. However, for some welding processes, the widths determined by microhardness profile and metallographic analysis may be different. This may be due to the mechanical properties of the parent metal adjacent to the weld which have changed as a result of heat input of the welding process. Meanwhile, the microstructure of the parent metal in the vicinity of the weld is free from the influence of the thermal cycle for the temperature does not reach the values that make the microstructure change. Therefore, the metallographic analysis must be combined with microhardness profile to obtain the width of the weld metal and HAZ accurately.

In the present research, the microhardness empirical formula and the improved rule of mixtures in conjunction with the mixed material and parent metal tensile tests configuration are applied to extract the mechanical properties of the weld metal, HAZ material, and parent metal in studying the formability of the QSTE340 welded tube. Based on ABAQUS platform, the FE method is employed to evaluate the contribution of the weld geometrical characteristic and mechanical properties on FE simulation results of the welded tube NC bending.

2 Materials and methods

The material used in this study is Nb–Ti microalloyed steel QSTE340. The welded tubes with the outside diameter D 78 mm and wall thickness t 2.7 mm are produced from flat sheet material by continuous roll forming and HF-ERW.

2.1 Material properties of the welded tube

2.1.1 Tensile test

Three standard uniaxial tensile testing specimens of the parent metal and three specimens of mixed material containing weld metal, HAZ material, and partial parent metal are cut from the welded tube. For the mixed material specimens, the weld line is located in the center of the tensile specimen and is oriented parallel to the load direction. Tensile test is performed using a CSS-44100 Electronic Universal Materials Testing Machine (100 KN, accuracy ±0.05 % of the indicated load) at a constant speed of 2 mm/min until necking occurred. The tensile properties for the QSTE340 parent metal and mixed material specimens are shown in Table 1.

2.1.2 Microhardness test

Vickers microhardness measurements are carried out in three zones of the weld region consisting of weld metal, HAZ, and parent metal using a HX-1000 microhardness tester produced by Shanghai Taiming Optical Instrument Co., Ltd. To improve measuring precision and reflect the microhardness throughout the entire zone across the weld, HAZ, and parent, the arc cross-sectional specimens are cut from the welded tube. Microhardness tests are done on the polished cross-sectional area; the Vickers hardness number are obtained by traveling the indenter in a straight path along the direction that is perpendicular to the weld line at an interval of 0.1 mm in the weld, 0.2 mm in the HAZ, and 1.0 mm in the parent with an indentation load of 300 gf for a duration of 15 s. Along the thickness direction, the hardness and width of the weld typically vary from the outside surface to the inside surface, so the average of six measurement points along the thickness direction is taken.

The microhardness distribution across the weld, HAZ, and parent metal of QSTE340 welded tube is shown in Fig. 2. As seen from the figure, it clearly shows the increased hardness in the weld compared with that of the parent metal and indicates that the HAZ extends over a distance of approximately ±10 mm from the center of the weld. The microhardness in the weld is greatest, the maximum reaches 210 HV, and that in the parent zone is the least, about 158 HV.

According to the distribution of microhardness across the weld, HAZ, and parent metal, the width of the weld is

Table 1 Mechanical properties of the QSTE340 parent metal and the mixed material

Parameters	Parent metal	Mixed material
Young's modulus, E (GPa)	218.518	236.582
Elongation percentage, δ (%)	32.2	26.4
Yield strength, $\sigma_{0.2}$ (MPa)	416.970	463.415
Ultimate tensile strength, σ_b (MPa)	467.642	495.665
Strength coefficient, K (MPa)	749.528	695.571
Hardening exponent, n	0.207	0.123
Anisotropy coefficient, R	0.765	0.884

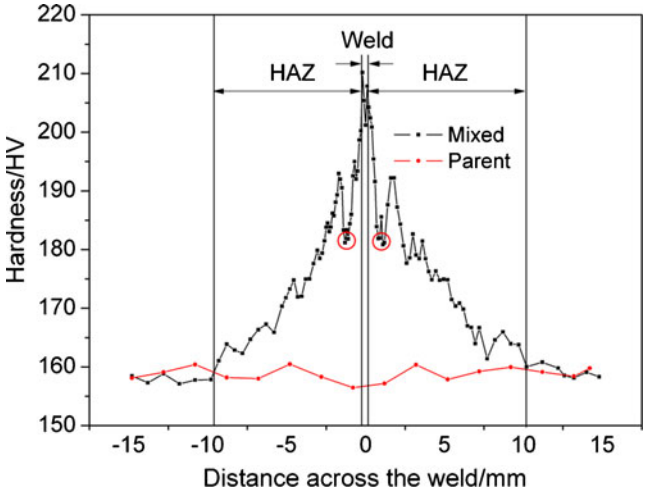

Fig. 2 Microhardness profile of the QSTE340 welded tube

determined as approximately 0.4 mm and that of each HAZ is about 9.0–10.0 mm.

2.1.3 Microstructure test

The arc cross-sectional specimens are cut from the welded tube, mounted, and polished as per standard metallographic procedures to observe the microstructure of the weld metal, HAZ, and parent metal. The polished specimens are etched with 3 % nital solution (3 ml HNO_3, 97 ml ethanol) for 20s and observed under an optical microscope.

The weld profile of the QSTE340 welded tube is observed as shown in Fig. 3. Note that the weld region is shaped like an hourglass. This is because the heat generated by the HF current enters the strip edge from the top and the side of the edge. The average width of the hourglass at the outside and inside surface of the welded tube is 2.9 mm; the width of the hourglass at neutral axis is about 2.7 mm; the area of the hourglass is about 7.435 mm^2. Since the average thickness of the weld region is 2.65 mm, the effective width of the weld is thus determined as b_w=2.8 mm, which is different from values obtained from the microhardness test method. It is found that the weld width obtained from the microstructure test is equal to the distance of the two troughs (the red open circles) of microhardness distribution, as shown in Fig. 2. Figure 3b displays the microstructure image of the weld area. The bright band in the center is the fusion zone, which is called the true weld [26]. It is seen that the weld consists of a narrow central weld of less than 0.5 mm, which is identical with the weld width obtained from the microhardness test.

The microstructures of the parent metal and weld region of QSTE340 welded tube under higher magnification are shown in Fig. 4. Figure 4a shows that the significant grain growth is observed in the center of the weld, and the grain is of irregular shape and size. Acicular ferrite and lamellar

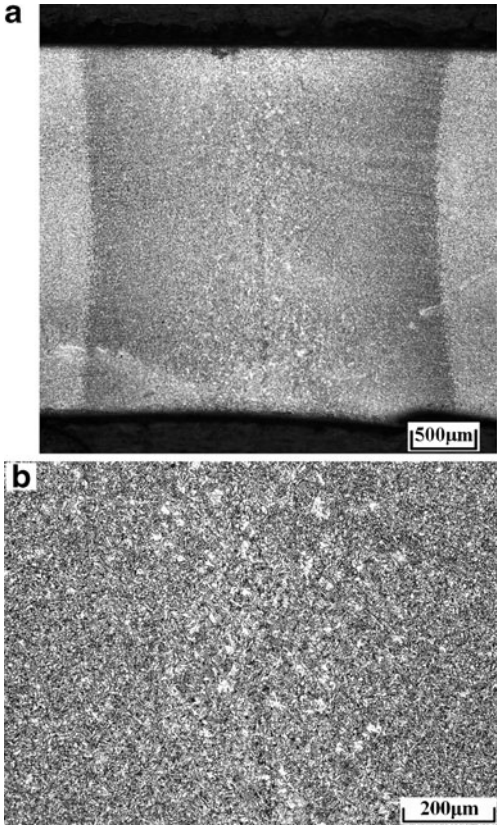

Fig. 3 The weld geometry of F-ERW welded tube: **a** weld region, **b** microstructure image of the weld area

pearlite are distributed in the weld. The development of the microstructures of the region that is 1.2 mm away from the weld centerline is represented by Fig. 4b; the grains are more equiaxed than those in the fusion zone, and the grain sizes in the weld region become smaller as the distance from the weld centerline increased and the influence of the heat is reduced. Meanwhile, the amount of grain growth increases rapidly as the weld fusion zone is approached, leading to the formation of the coarse-grained microstructural region. Figure 4c depicts the visible boundary between the weld region and parent metal; the fine-grained region of the weld metal is shown on the left of the figure and those of the parent on the right. It clearly indicates that the distinct change in grain size and rapid transformation between the grains of the weld metal and the parent due to the gradient of thermal conduction and the changes in the grain structure compare well with the rapid reduction in hardness (red open circles in Fig. 2). Figure 4d shows the microstructure of the parent metal, which is composed of equiaxed ferrite grains; small regions of pearlite are present in the parent metal microstructure at grain boundary edges and corners.

By analyzing the microstructure image and microhardness distribution of the weld region of the QSTE340 welded tubes, the width of the weld is calculated. In the first case, the width of the weld is determined by the obvious variation of

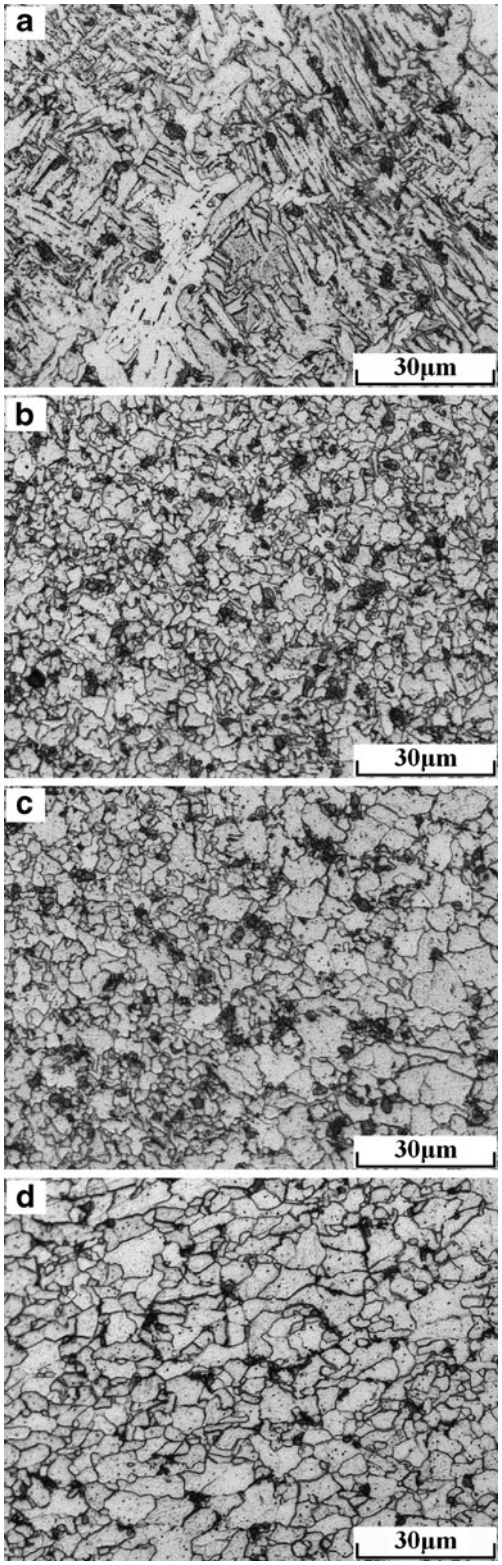

Fig. 4 Microstructure observed in the cross-section of QSTE340 welded tube: **a** fusion region, **b** 1.2 mm away from the fusion line, **c** boundary of weld region and parent, **d** parent metal

microstructures, so the weld width is determined as b_w= 2.8 mm, which is identical with the rapid reduction in hardness (red open circles in Fig. 2); in the second case, the fusion line is considered to be the weld, so the weld width is determined as b_w=0.4 mm, which is identical with the weld width obtained from the microhardness test. However, the width of the HAZ cannot be determined from the microstructure. The HAZ is the transition zone between the fusion zone and the parent metal. The varying mechanical properties and the microstructure of the heterogeneous HAZ are the result of the non-uniform heat treatment applied during the weld thermal cycle. Regions closest to the fusion zone experience the highest temperatures and the fastest cooling rates. The mechanical properties of the parent metal that is adjacent to the weld have changed; however, the microstructure of the parent metal near the weld is free from the influence of the thermal cycle for the temperature does not reach the values that make the microstructure change. This can be proved by Fig. 4c, d; the microstructure of the parent metal in Fig. 4d is the same as the microstructure of the HAZ material on the right of Fig. 4c. Therefore, a quantitative description of the HAZ width is provided by its microhardness profile. The approximate boundaries of the parent and HAZ are delineated in Fig. 2, and the total width of the weld region including the weld and HAZ is determined as b_h=19.4 mm.

2.1.4 The relation of the weld metal and HAZ of the welded tube

The constitutive relationship of QSTE340 welded tube is obtained based on microhardness empirical formula [18] and improved rule of mixtures [23], as shown in Eqs. (1), (2), and (3).

$$\sigma_y^{weld} = \sigma_y^{parent}\frac{HV_w}{HV_p};\quad \sigma_y^{haz} = \sigma_y^{parent}\frac{HV_h}{HV_p} \tag{1}$$

where HV represents the microhardness, σ_y represents the yield stress, and the subscripts w, h, and p refer to the weld metal, HAZ, and parent metal, respectively.

$$\sigma_w = \frac{A_m(HV_w - HV_p)}{A_w(HV_w - HV_p) + A_h(HV_h - HV_p)} \times (\sigma_m - \sigma_p) + \sigma_p \tag{2}$$

$$\sigma_h = \sigma_p + \frac{HV_h - HV_p}{HV_w - HV_p}(\sigma_w - \sigma_p) \tag{3}$$

where A represents the area, and the subscript m refer to the mixed material.

The average width of the weld observed in the microhardness and microstructure test is about 0.4 and

2.8 mm, respectively; the total width of the weld region including the weld and HAZ is approximately 19.4 mm. Due to the nonsymmetrical nature of the welding process, the width of HAZ is not symmetric with respect to the weld centerline. So, the average width of HAZ and the values of microhardness in the weld, HAZ, and parent metal are given in Table 2; the areas of the cross-section of the weld and HAZ of QSTE340 welded tube are obtained according to the metallographic section, the width and thickness of the HAZ. Then, substitute the stress of parent metal and mixed material, the area, and the microhardness of weld metal, HAZ, and parent metal into Eqs. (1), (2), and (3). The strength coefficient K and strain hardening exponent n of weld metal and HAZ of QSTE340 welded tube based on different constitutive relation are obtained, as presented in Table 2. It is found that the weld metal has minimal K and n based on improved rule of mixtures. K corresponds with the microhardness values and n is the same in each zone based on microhardness empirical formula.

2.2 Weld profile

Generally speaking, regardless of the frequency of the power source used to make longitudinal butt welds in tube, a discernible hourglass shape signature is present when the HF-ERW process is used. In order to evaluate the effects of weld profile on the deformation behaviors of the weld region, two typical cross-sections of the HF-ERW weld geometry are considered.

The first case deals with the weld according to the true form of the weld profile, and the size of the weld is acquired metallographically in the macro condition, as shown in Fig. 5.

The second case reduces the weld to a sectorial weld profile. The width of the weld is determined according to the assumption that the hourglass and sectorial weld profile have equal volume of weld material, so the sectorial angle of the sector is 4.19°, as shown in Fig. 6.

2.3 Establishment of FE models for NC bending of welded tube

3D FE model is established to simulate the welded tube NC bending process using ABAQUS/Explicit, as shown in Fig. 7. In order to numerically describe the effects of weld characteristics on the forming quality of the welded tube in NC bending process, two types of welded tube in FE model are employed, i.e., 3D solid element model with weld and HAZ, wherein the weld profile is sectorial (shortened as model-WSS), and 3D shell element model with weld and HAZ (shortened as model-WS), and for the models that include the weld, the weld width is 2.8 mm.

The whole bending process of welded tubes includes bending, ball retracting, and unloading. The explicit dynamic FE code is applied to simulate the tube bending and retracting processes. The universal flexing mandrel is modeled as comprising a mandrel shank and two flexible balls; the link between the mandrel shank and the first mandrel ball and successive flexible balls is modeled by a "connector element". Hill anisotropic quadratic yield function is used to describe the thickness anisotropic plasticity.

For contact pairs, the "surface-to-surface contact" method is used to define the contact conditions. For different contact interfaces, Coulomb friction law is chosen to represent the friction behaviors between tube and dies. The boundary constraints and loading paths are applied by "velocity/angular".

For one specific forming process, the determinations of the number of elements, element shapes, and element types are very important to get more precise results based on reasonable computational fees. In this study, 3D linear reduced integration continuum elements with eight nodes and hourglass control R3D8R are used to model the solid tube; also the four-node doubly curved thin shell S4R is used to model the shell tube. The relatively rigid tools are treated as

Table 2 The width, average microhardness, and material properties based on improved rule of mixtures and microhardness empirical formula for different zones of QSTE340 welded tube

Zone		b_w=0.4 mm			b_w=2.8 mm		
		Parent	HAZ	Weld	Parent	HAZ	Weld
Width (mm)			9.5	0.4		8.3	2.8
Microhardness (HV)		158.809	178.751	205.771	158.809	175.151	191.932
Improved rule of mixtures	K (MPa)	749.528	732.109	645.871	749.528	709.489	670.985
	n	0.2069	0.1790	0.0183	0.2069	0.1375	0.0629
Microhardness empirical formula	K (MPa)	749.528	800.927	870.772	749.528	791.597	834.973
	n	0.2069	0.1930	0.1769	0.2069	0.1954	0.1848

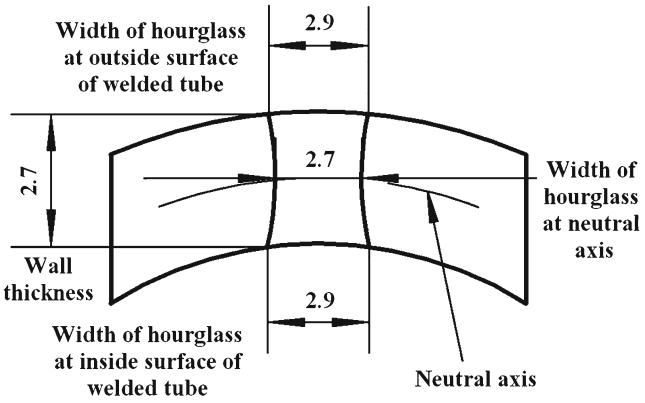

Fig. 5 Schematic of the welded tube with an hourglass weld profile

discrete rigid bodies with four-node 3D bilinear quadrilateral rigid element R3D4.

Additionally, the tube is divided into weld zone, HAZ, and parent zone for the models including weld and HAZ, and each is assigned corresponding mechanical properties. The mechanical constitutive relations of the welded tube are shown in Table 2. For simplification, the weld and subdivided HAZs are symmetrical about the weld centerline. The different forming parameters are shown in Table 3.

2.4 Experiment equipment and conditions

To validate the established FE models, comparisons between the FE simulation and experimental results are carried out with respect to the strain variations and cross-sectional deformation. According to Fig. 1, the weld locates on the outside of the bend as the weld angle is 0°, in the middle as the weld angle is 90° and 270°, and inside as the weld angle is 180°.

The experiments are carried out using a GQ W27YPC-159 PLC hydraulic bender, as shown in Fig. 8. The experimental conditions are the same as in the simulation, as shown in Table 3. The push assistant level is defined as

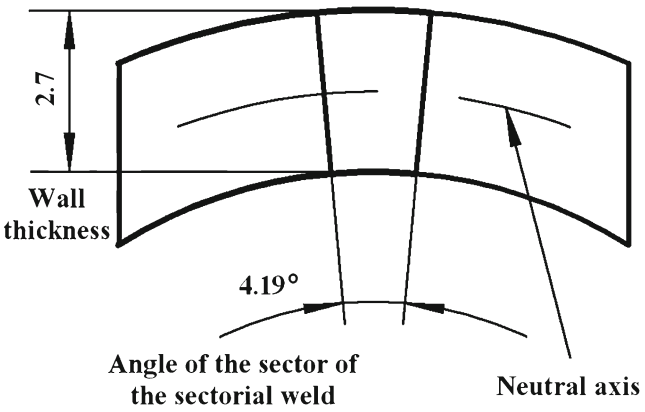

Fig. 6 Schematic of the welded tube with a sectorial weld profile

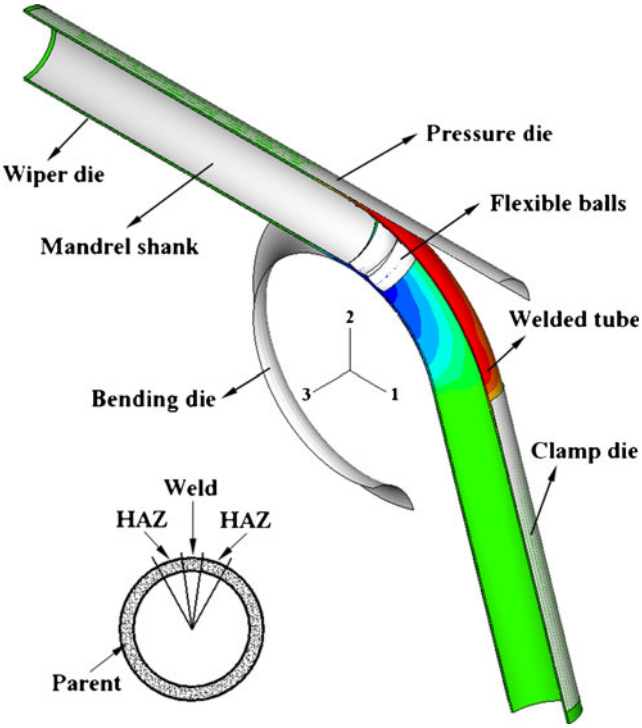

Fig. 7 3D FE model for NC bending of welded tube

the ratio of the speed of the pressure die V_p to the instant tangential linear speed V_b measured at the centerline bending radius of bend die ($V_b = \omega R_d$). The QSTE340 welded tube bending is conducted.

2.5 Forming quality index

The key deformation behaviors of welded tube in terms of wall thinning degree Δt_{out}, wall thickening degree

Table 3 Forming parameters for different bending sizes

Forming parameters	Values		
Tube outside diameter, D (mm)	60	78	100
Wall thickness, t (mm)	4.0	2.7	1.7
Weld width, (mm)	1.89	2.8 (0.4)	4.45
Total HAZ width, (mm)	11.205	16.6 (19)	26.36
Bending radius, R_d (mm)	120	156	200
Mandrel diameter, d (mm)	51	71.9	96.2
Ball diameter, d_0 (mm)	50.9	71.8	96.1
Ball thickness, k (mm)	20	25	25
Number of balls, N	2	2	3
Mandrel extension length, e (mm)	5	5	5
Final bending angle, (rad)	π/2	π/2	π/2
Push assistant level, (%)	100	100	100

Fig. 8 NC hydraulic tube bender W27YPC-159 and the formed QSTE340 welded tube

Δt_{in}, and cross-sectional deformation degree ΔD are described as follows:

$$\Delta t_{out} = \frac{t'_{out} - t}{t} \times 100\% \quad (4)$$

$$\Delta t_{in} = \frac{t'_{in} - t}{t} \times 100\% \quad (5)$$

where t is initial tube wall thickness, t'_{out} is the wall thickness outside the bend after bending, and t'_{in} is the wall thickness inside the bend after bending, as shown in Fig. 9.

$$\Delta D = \frac{D - D'}{D} \times 100\% \quad (6)$$

where D is initial tube outer diameter, D' is the cross-section length in the vertical direction after bending, as shown in Fig. 9.

2.6 Verification of the FE models

To validate the established FE models, comparisons between the FE and experimental results are carried out with respect to the wall thinning, wall thickening, and cross-sectional deformation degree. The weld locates on the outside of the bend, and the improved rule of mixtures is adopted to describe the mechanical constitutive relations of the welded tube. Figure 10 shows the comparison results. In terms of the maximum Δt_{in}, it is found that the relative errors between experiment and simulation for model-WSS and model-WS are less than 6.03 and 0.71 %, respectively. As for the maximum Δt_{out}, the relative errors are less than 2.37 and 1.70 %, respectively. For the maximum ΔD, the relative errors are less than 13.05 and 10.16 %, respectively. The overall comparison of the FEA results with the experimental ones shows that the established FE models are reliable.

3 Results and discussion

3.1 Effects of the mechanical constitutive relations

Figure 11 shows the predicted strain distributions along the mid-cross-section of welded tube with different mechanical constitutive relationships. 3D shell element model with weld and HAZ is used to simulate the welded tube NC bending process, the weld line locates on the outside, and the weld width is 2.8 mm; the weld and HAZ are within 0~14.76°. In order to testify the computational accuracy of different mechanical constitutive relationships for welded tube NC bending, the experimental results are also illustrated in the figure. The maximum relative errors of simulated tangent strain, hoop strain, and thickness strain determined by the improved rule of mixtures and microhardness empirical formula are 1.33 and 1.75 %, 17.60 and 24.95 %, and 3.25 and 5.95 %, respectively, as compared with the experimental results. The overall comparison of the FE results with the experimental ones shows that the established FE models are reliable, and the predicted results of FE model based on improved rule of mixtures have a good agreement with the ones from the experiments as compared with that based on the microhardness empirical formula.

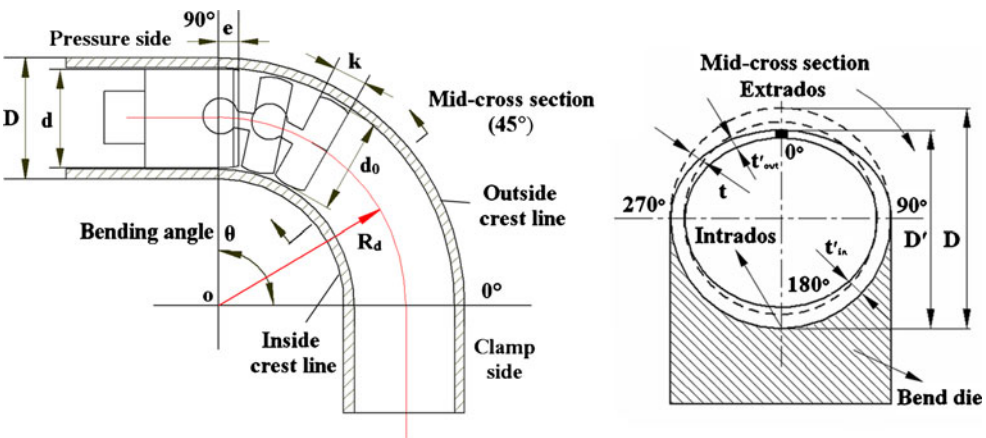

Fig. 9 Schematic diagrams of measuring positions for tube bending deformation

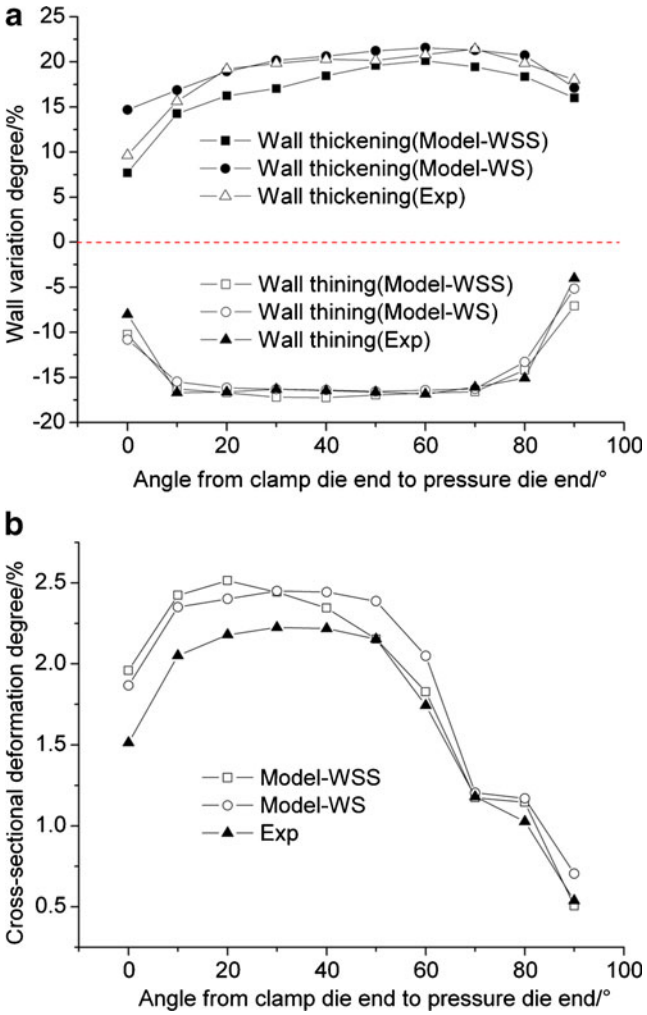

Fig. 10 Comparisons of wall variations and cross-sectional deformation degrees between FE and experiment: **a** wall thinning and wall thickening along the extrados and intrados, **b** cross-sectional deformation

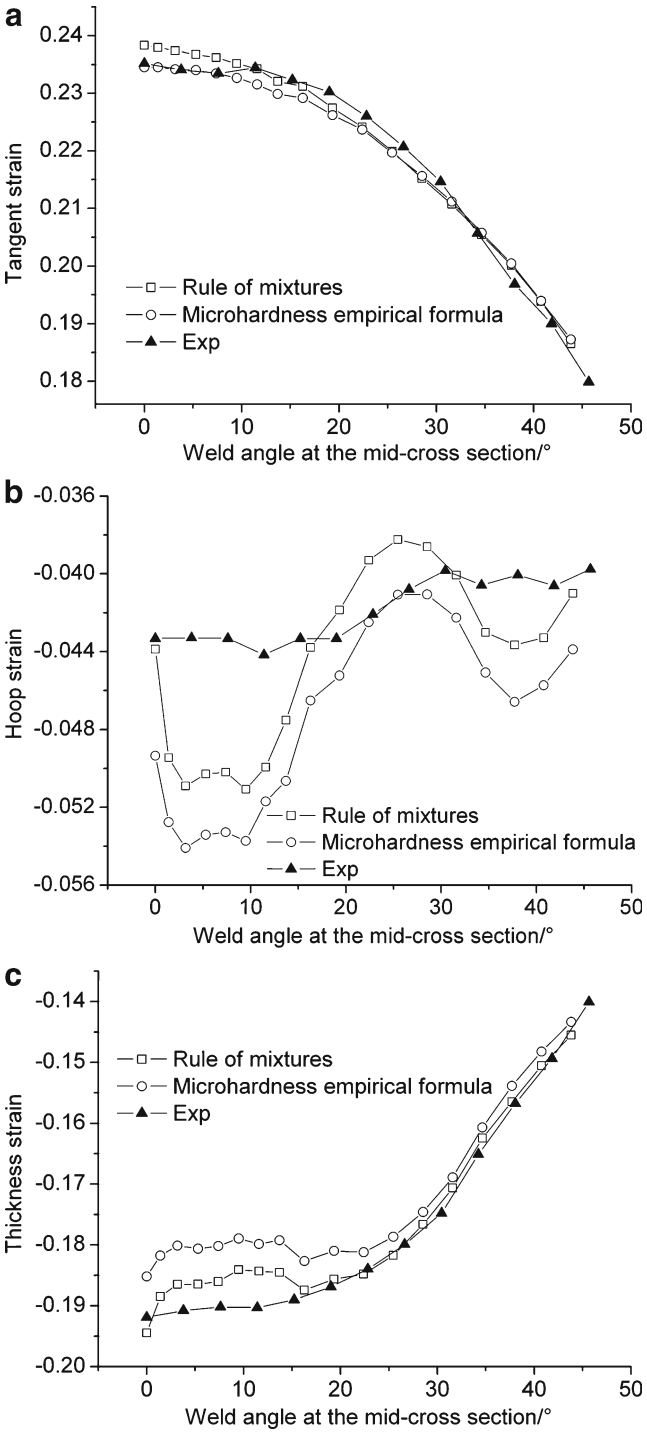

Fig. 11 Predicted and experimental strain distributions along the mid-cross section of welded tube with different constitutive relationships: **a** tangent strain, **b** hoop strain, **c** thickness strain

As can be seen from Fig. 11, the tangent strain and thickness strain determined by the microhardness empirical formula decreases obviously in the weld and HAZ as compared with that determined by the improved rule of mixtures. On the contrary, the hoop strain becomes larger in the weld and HAZ. The variation trend is almost the same for the two cases. The maximum relative discrepancies of tangent strain, hoop strain, and thickness strain of the two models are 1.62, 12.49, and 5.01 %, respectively. As seen from Table 2, the flow stresses of the weld and HAZ determined by the microhardness empirical formula are higher than that determined by the improved rule of mixtures in the large deformation condition; it will decrease the deformation capacity of the weld region. The larger relative discrepancies of hoop strain indicate that the weld metal undergo more deformation along the hoop direction, which is similar to the welded tube hydroforming wherein the initial fracture took place on HAZ near the welding line [27]. Meanwhile, the differences of the tangent strain and thickness strain are gradually diminishing for the parent metal away from the weld region; this is because of the higher hardening behaviors of the weld and HAZ material impose a stronger constraining effect on the deformation of the weld region. There is another important factor in that the hardening behaviors of the weld and HAZ material

determined by the microhardness empirical formula are almost identical to the parent metal, and that was not in accordance with the fact [22], for the material properties are continuous changes from the weld center to the parent. Therefore, the improved rule of mixtures is used, which can demonstrate the forming features of the welded tube well.

Figure 12 shows the comparison between simulation and experimental cross-sectional deformation degree with different mechanical constitutive relationships. It can be seen that the ΔD distributions determined by the microhardness empirical formula are close to the experimental ones, and the ΔD determined by the improved rule of mixtures is larger than that determined by the microhardness empirical formula. The maximum relative errors of simulated maximum ΔD determined by the improved rule of mixtures and microhardness empirical formula are 10.16 and 8.87 % as compared with the experimental results. All things considered, the selection of the improved rule of mixtures is reasonable in this paper.

3.2 Effects of the weld width determined by different methods

As was noted earlier, the weld may play a crucial role in the tube failure during NC bending of welded tubes, especially as the weld line locates on the outside of the bend. Since the average width of the weld observed in the microhardness and microstructure test is 0.4 and 2.8 mm, to further investigate the effect of the weld width determined by the microhardness and microstructure test on the deformational behaviors of welded tube, FE simulations are performed by varying the weld width; the rule of mixtures is adopted to determine the constitutive relationship of different zones of QSTE340 welded tube, as shown in Table 2. 3D shell element model with weld and HAZ is used to simulate the NC bending process of welded tube; the weld and HAZ are within 0–14.76°.

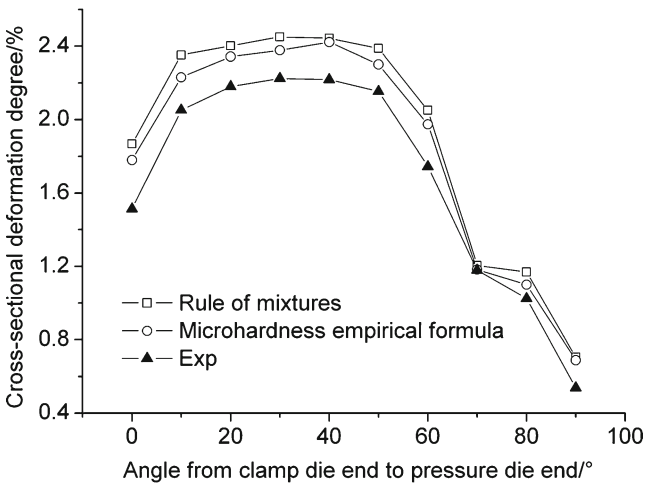

Fig. 12 Cross-sectional deformation distributions with different constitutive relationships

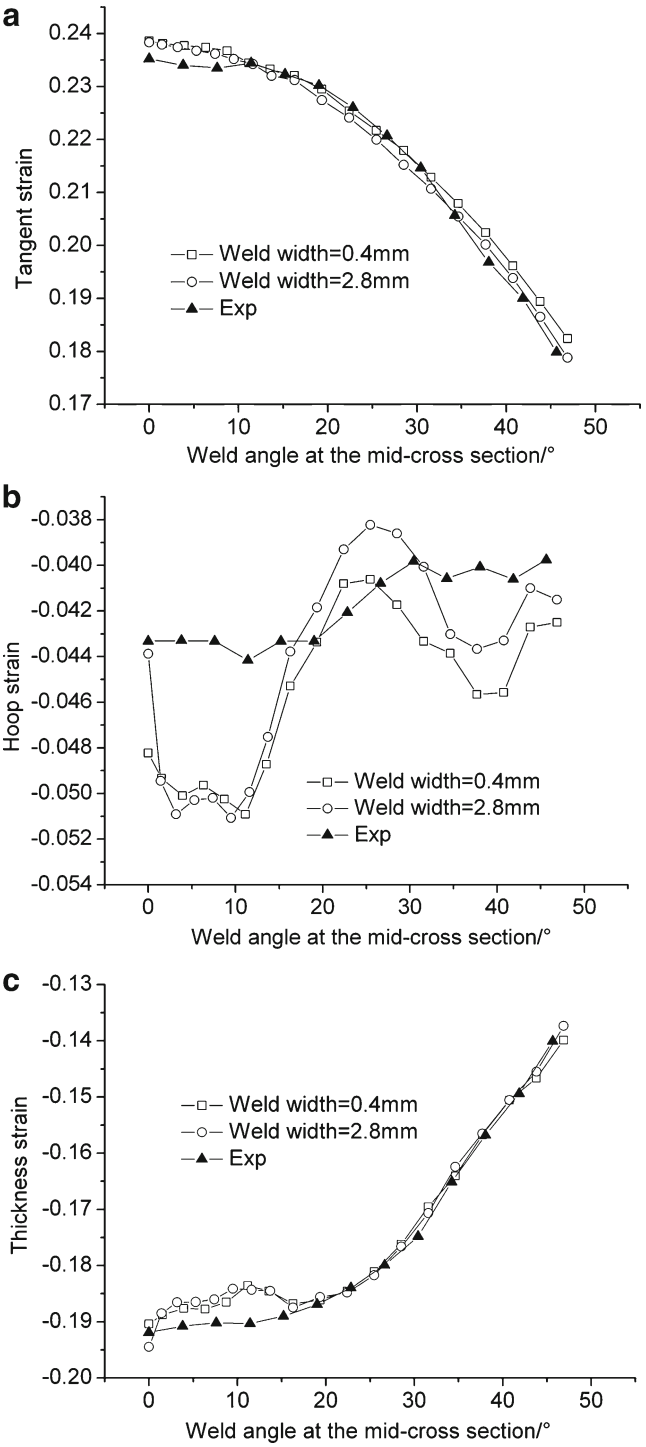

Fig. 13 Predicted strain distributions along the mid-cross-section of welded tube with different weld widths: **a** tangent strain, **b** hoop strain, **c** thickness strain

Figure 13 shows the comparison between experimental and predicted strain distributions along the mid-cross-section of the welded tube with different weld widths. The

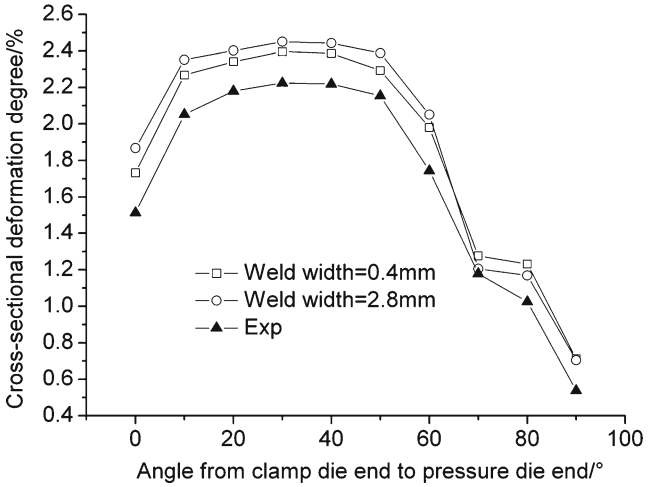

Fig. 14 Cross-sectional deformation distributions with different weld widths

maximum relative errors of simulated tangent strain, hoop strain, and thickness strain determined by 0.4 and 2.8 mm weld width are 2.83 and 1.33 %, 15.73 and 17.60 %, and 3.53 and 3.25 %, respectively, as compared with the experimental results. The overall comparison of the FE results with the experimental ones shows that the weld widths determined by the microhardness and microstructure test almost have little effect on the deformational behaviors of the welded tube. However, for the same computational condition, the FE model with 0.4 mm weld width increases the computing time dramatically. The CPU time for FE model with 0.4 mm weld width is almost 2.2 times as that for FE model with 2.8 mm weld width.

Figure 13a shows that the tangent strains predicted in the FE model with a narrow weld are slightly higher than the strains measured in the FE model with a wider weld zone; the relative discrepancies are less than 2.01 %. The comparisons show that the different weld widths determined by the microhardness and microstructure test have a negligible effect on tangent strain distribution. Figure 13b shows that the hoop strain distribution is entirely non-uniform along the mid-cross-section of the welded tube, and the hoop strain in HAZ is much higher than the strain in the weld and parent zone, which indicates that the HAZ material undergoes more deformation along the hoop direction. A significant gradient of the strain distribution happens between two neighboring elements of the weld metal and the HAZ due to the sudden changes of the mechanical properties; the same phenomenon is observed between the HAZ and the parent metal. As the weld width changes from 0.4 to 2.8 mm, the hoop strain decreases by 9.02 % at the extrados and the discrepancies are little in HAZ. Figure 13c shows that the calculated thickness strain distribution is non-uniform in the weld and HAZ, and the strains in the parent metal that is adjacent to the

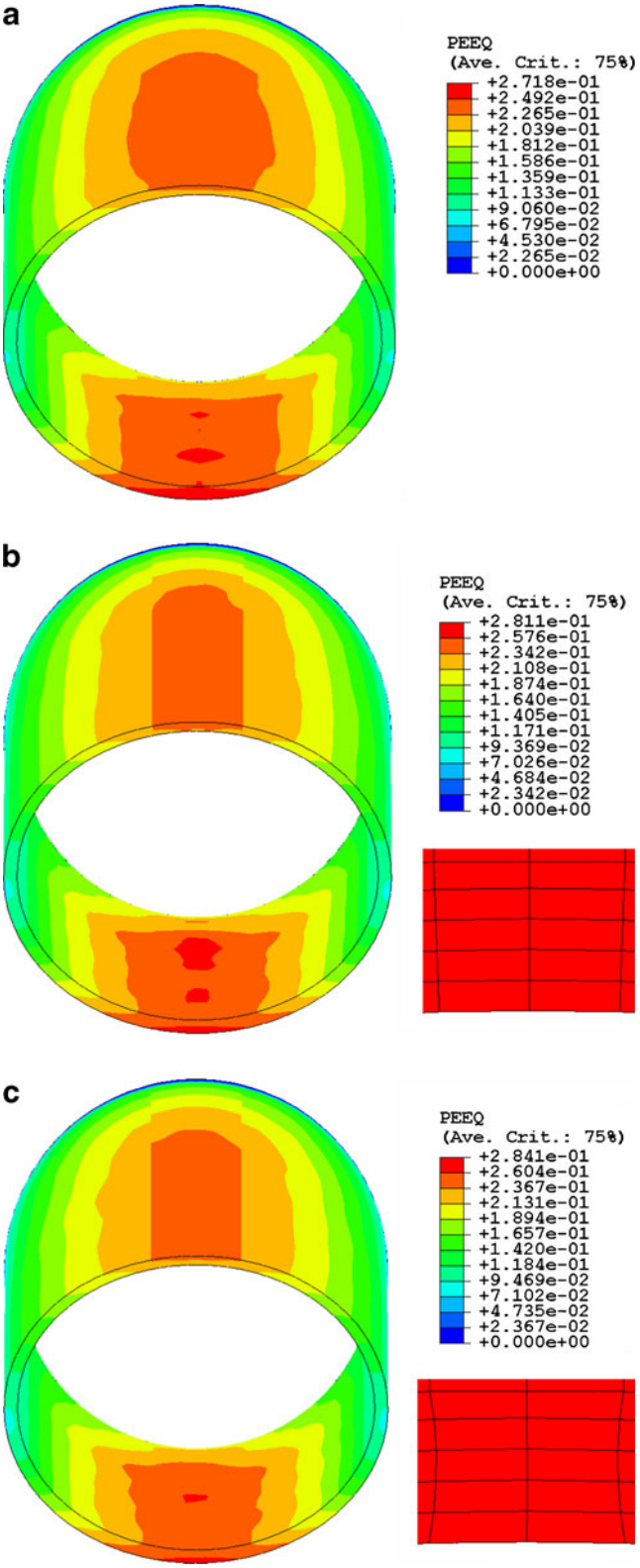

Fig. 15 Equivalent plastic strain distributions with different weld profiles: **a** model-PCS, **b** model-WSS, **c** model-WSH

HAZ are already higher than those in the HAZ but smaller than those in the weld metal. The thickness

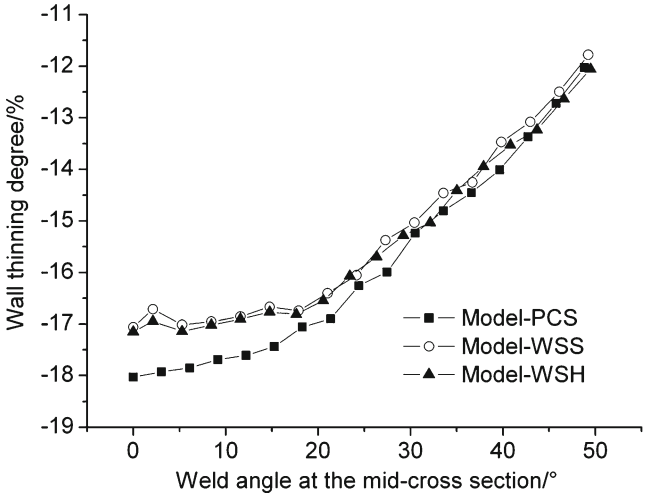

Fig. 16 Predicted wall thinning distributions along the mid-cross-section of the welded tube

strain of the FE model with 0.4 mm weld width becomes smaller at the extrados in contrast with the FE model with 2.8 mm weld width. As seen from Table 2, the average hardness of the weld is 205.771 HV as the weld width is 0.4 mm, while the average hardness of the weld is 191.932 HV as the weld width is 2.8 mm; the higher hardness will decrease the ductility and plastic deformation capacity, thus leading to a lower thickness strain in the weld. The average hardness of the HAZ is almost identical for the two models, so the differences of thickness strain are little in the HAZ.

Figure 14 shows the comparison between the simulation and experimental cross-sectional deformation with different weld widths. It can be seen that the ΔD determined by the FE model with 2.8 mm weld width is larger than that determined by the FE model with 0.4 mm weld width. The maximum relative errors of simulated maximum ΔD determined by 0.4 mm weld width and 2.8 mm weld width are7.72 and 10.16 % as compared with the experimental results. The comparison shows that weld widths determined by the microhardness and microstructure test have little effect on the ΔD.

3.3 Effects of the weld profile and properties

In order to investigate the effects of the weld characteristics on the forming behaviors in the welded tube NC bending process, FE simulations are performed by systematically varying the weld profile and weld material properties under certain imposed conditions. Therefore, a 3D solid element model with weld and HAZ is established, and the weld profile is hourglass (shortened as model-WSH); a 3D solid element model with continuous parent metal (shortened as model-PCS) is also established for comparison. To assess the effects of weld profile on the forming behaviors of the welded tube, there should be a comparison between the model-WSH and model-WSS, and in this comparison, the elements that represent the weld locate on the outside of the bend.

Figure 15 shows the distributions of the equivalent plastic strain of model-PCS, model-WSS, and model-WSH. It is found that the implementation of the weld profile and weld material properties increases the maximum equivalent plastic strain; the maximum relative discrepancy is 4.53 % as compared with model-PCS. The results showed that model-WSS and model-WSH predicted almost the same equivalent plastic strain distributions on the outside of the bent tube; however, a significant gradient of equivalent plastic strain distribution happens at the interface of the HAZ material and parent metal due to changes of the mechanical properties.

In order to numerically determine the effect of the weld profile and weld material properties on the forming quality of the welded tube, the wall thinning, thickening distributions along the mid-cross-section of the welded tube, and the cross-sectional deformation are compared among the three cases. Figure 16 shows the wall thinning distributions of model-PCS, model-WSS, and model-WSH along the mid-cross-section of the welded tube. Table 4 shows the wall thinning values at the extrados.

The results show that the predicted wall thinning on the outside of the bent tube is influenced by the weld profile and weld material properties, and when the weld profile and material properties are ignored, the model-PCS has the largest wall thinning at the extrados, the maximum wall thinning is −18.03 %, and an entirely uniform trend along the hoop direction is observed.

When the weld profile and weld properties are considered, the implementation of weld profile and weld properties in FE models decreases the wall thinning dramatically in the weld and HAZ; the FE model with the sectorial weld profile and weld properties has minimal wall thinning. The wall thinning of model-WSS and model-WSH decrease by 5.38 and 4.88 % as

Table 4 Wall variations at the extrados and intrados

	Wall thinning/%	Difference/%	Wall thickening/%	Difference/%
Model-PCS	−18.03	Base	19.69	Base
Model-WSS	−17.06	5.38	18.03	−8.43
Model-WSH	−17.15	4.88	18.34	−6.86

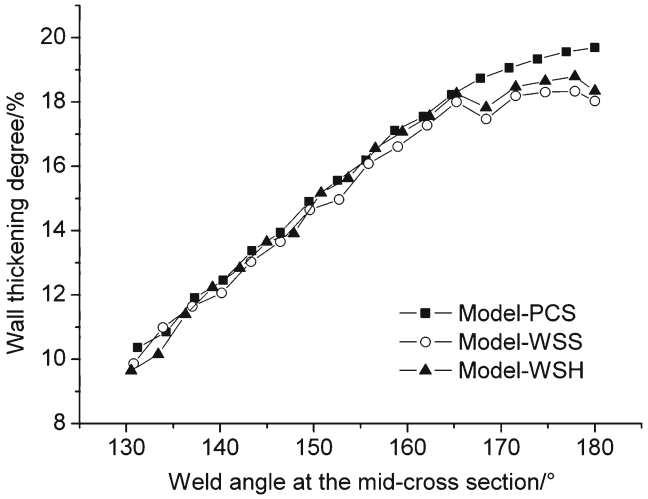

Fig. 17 Predicted wall thickening distributions along the mid-cross section of welded tube

compared with model-PCS; this is most likely due to the lower ductility and plastic deformation capacity of the weld region. Also, it indicates that the sectorial weld profile has a stronger impact on wall thinning than the hourglass profile, and the differences of wall thinning are gradually diminishing from the weld to the parent; it indicates that the constraining effect of the parent metal on the weld region is gradually decreasing with the increase of the weld angle. An obvious gradient of the wall thinning distribution happens at the interface of the weld profile, HAZ, and parent; this may be attributed to the strain localization at the interface. The entire variation trend of the two cases is the same along the hoop direction. The discrepancies of wall thinning of the three models are little in the parent metal as the angle is greater than 24°; it indicates that the constraining effect of weld profile and weld properties is little on the parent metal away from the weld region.

Figure 17 shows the wall thickening distributions along the mid-cross section of the welded tube of three models. Table 4 shows the wall thickening values at the intrados. The weld line locates on the inside; the weld and HAZ are within 165.24–180°.

The results show that the predicted wall thickening distributions on the inside of the bent tube of the weld region are influenced by the weld profile and weld material properties. When the weld profile and material properties are ignored, the model-PCS has the largest wall thickening at the intrados, the maximum wall thickening is 19.69 %, and the variation trend is uniform along the hoop direction.

When the weld profile and weld properties are considered, the implementation of weld profile and weld properties in FE models decreases the wall thickening dramatically in the weld and HAZ; the wall thickening of model-WSS and model-WSH decrease by 8.43 and 6.86 % as compared with model-PCS. It indicates that the sectorial weld profile has a stronger impact on the wall thickening than the hourglass profile. An obvious gradient of the wall thickening distribution happens at the interface of the weld profile, HAZ, and parent. The entire variation trend of the two cases is the same along the hoop direction. The discrepancies of the three models are little in the parent metal as the angle is less than 165°; it indicates that the constraining effect of the weld profile and weld properties is little on the parent metal away from the weld region.

Table 5 shows the maximum cross-sectional deformation with different FE models. The results show that the implementation of weld profile and weld properties in FE models increases the maximum cross-sectional deformation value. As the weld line locates on the outside, the largest cross-sectional deformation is observed for the model with the sectorial weld profile and weld properties, and the sectorial weld profile has a stronger effect on the increase of maximum cross-sectional deformation than the hourglass profile.

As the weld line locates on the inside, the largest cross-sectional deformation is observed for the model with the sectorial weld profile and weld properties. The effect of the sectorial weld profile on the increase of maximum cross-sectional deformation is more significant compared with that of the weld line which locates on the outside.

3.4 Effects of the same weld volume under different D/t

To further investigate the effects of the same weld volume under different D/t on the forming quality of the bent welded

Table 5 Predicted maximum cross-sectional deformation with different FE models

	Maximum cross-sectional deformation/%(weld-outside)	Difference/ %	Maximum cross-sectional deformation/%(weld-inside)	Difference/ %
Model-PCS	2.37	Base	2.37	Base
Model-WSS	2.52	6.33	2.56	8.02
Model-WSH	2.45	3.38	2.45	3.38

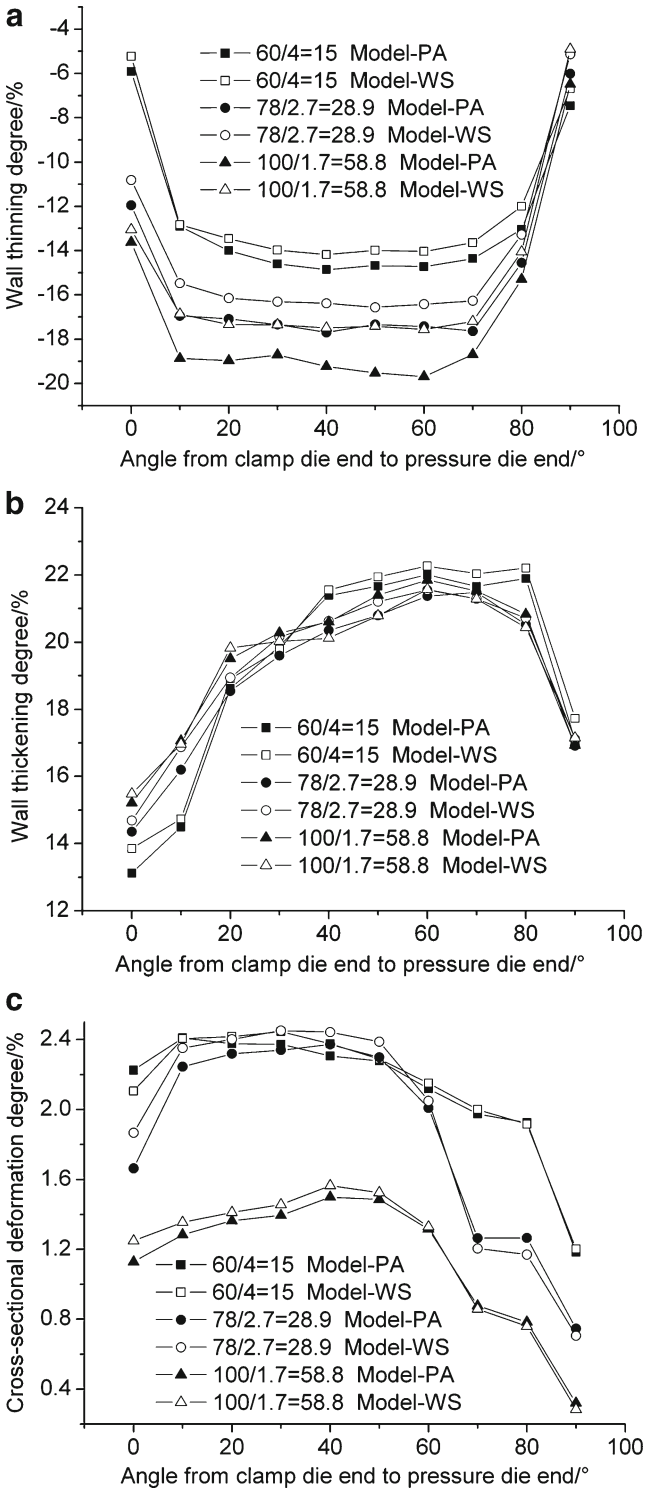

Fig. 18 Comparisons of wall variations and cross-sectional deformation degrees with different wall factors: **a** wall thinning along the extrados, **b** wall thickening along the intrados, **c** cross-sectional deformation

tube, the relationships between the model-WS and 3D shell element model with parent alone (shortened as model-PA) for the wall variation and the cross-sectional deformation are studied under three different wall factors D/t, including 15(60×4.0), 28.9(78×2.7), and 58.8(100×1.7). The model-WS with different D/t have the same weld and HAZ volume for accurate comparison; the weld line locates on the outside. The detailed simulation conditions are shown in Table 3.

Figure 18a shows that, with larger D/t, the wall thinning degree increases greatly. For the same D/t, the implementation of weld details in FE models decreases the wall thinning dramatically compared with model-PA. As the D/t increases from 15 to 28.9, the relative discrepancies of maximum wall thinning between the model-WS and model-PA change from 4.78 to 6.88 %, while the relative discrepancies are less than 12.12 % as the D/t is 58.8. It indicates that the same weld volume has a larger effect on wall thinning with larger D/t.

Figure 18b shows that the maximum wall thickening at the intrados with larger D/t is nearly similar, and the implementation of weld details in FE models has a negligible effect on the wall variation at the inside of the bent tube. The relative discrepancies of maximum wall thickening between the model-WS and model-PA are 0.37, 1.18, and 1.26 % as the D/t is 15, 28.9, and 58.8, respectively, which indicates that the effect of the same volume on wall thickening with different D/t can be ignored.

Figure 18c shows that the cross-sectional deformation becomes smaller progressively as the D/t increases from 15 to 28.9, while when D/t exceeds 28.9, the maximum cross-sectional deformation decreases sharply. The implementation of weld details in FE models increases the cross-sectional deformation. The relative discrepancies of maximum cross-sectional deformation between the model-WS and model-PA increase with larger D/t; it indicates that the same weld volume has a larger effect on the cross-sectional deformation with larger D/t.

4 Conclusions

The effect of weld characteristics on the formability of welded tubes in NC bending process is numerically investigated by finite element method. The results are shown as follows:

1. The predicted results of FE model based on the improved rule of mixtures are in good agreement with the ones from the experiments as compared with that based on the microhardness empirical formula. The tangent strain, thickness strain, and ΔD distribution determined by the microhardness empirical formula decrease obviously in weld and HAZ as compared with that determined by the improved rule of mixtures, which is contrary to the hoop strain. Meanwhile, the differences of the tangent strain and thickness strain are gradually diminishing for the parent metal away from the weld region.

2. The different weld and HAZ widths determined by the microhardness profile and metallographic section have a little effect on the tangent strain, thickness strain, and ΔD distribution. The hoop strain predicted in the model with a narrow weld becomes larger at the extrados in contrast with the strain measured in the model with a wider weld zone, and the discrepancies are little in HAZ.
3. The implementation of weld profile and material properties decreases the wall variation of the weld region as the weld line locates on the outside and inside. On the contrary, both the weld profile and weld material properties increase the maximum ΔD. The sectorial weld profile has a stronger impact on wall variation and maximum ΔD than the hourglass profile. The effect of the sectorial weld profile on the increase of maximum cross-sectional deformation is more significant compared with that when the weld line locates on the outside.
4. With larger D/t, the same weld and HAZ volume have a stronger effect on wall thinning and ΔD, and the effect on wall thickening with different D/t can be ignored.

Acknowledgments The authors would like to thank the National Natural Science Foundation of China (50875216) and 111 project (B08040) for financial support of this research.

References

1. Koc M, Altan T (2001) An overall review of the tube hydroforming (THF) technology. J Mater Process Technol 108:384–393
2. Hashmi MSJ (2006) Aspects of tube and pipe manufacturing processes: meter to nanometer diameter. J Mater Process Technol 179:5–10
3. Panda SK, Ravi Kumar D (2009) Study of formability of tailor-welded blanks in plane-strain stretch forming. Int J Adv Manuf Technol 44:675–685
4. Yang H, Yan J, Zhan M, Li H, Kou YL (2009) 3D numerical study on wrinkling characteristics in NC bending of aluminum alloy thin-walled tubes with large diameters under multi-die constraints. Comput Mater Sci 45:1052–1067
5. Panda SK, Ravi Kumar D (2010) Experimental and numerical studies on the forming behavior of tailor welded steel sheets in biaxial stretch forming. Mater Des 31:1365–1383
6. Kim J, Kim YW, Kang BS, Hwang SM (2004) Finite element analysis for bursting failure prediction in bulge forming of a seamed tube. Finite Elem Anal Des 40:953–966
7. Bhagwan AV, Kridli GT, Friedman PA (2002) Influence of weld characteristics on numerically predicted deformation behavior of aluminum tailor welded blanks. SAE, Paper No. 2002-01-0386
8. Panda SK, Ravi Kumar D, Kumar H, Nath AK (2007) Characterization of tensile properties of tailor welded IF steel sheets and their formability in stretch forming. J Mater Process Technol 183:321–332
9. Yu ZH, Yan HG, Gong XS, Quan YJ, Chen JH, Chen Q (2009) Microstructure and mechanical properties of laser welded wrought ZK21 magnesium alloy. Mater Sci Eng A 523:220–225
10. Hamidinejad SM, Hasanniya MH, Salari N, Valizadeh E (2013) CO_2 laser welding of interstitial free galvanized steel sheets used in tailor welded blanks. Int J Adv Manuf Technol 64:195–206
11. Imaninejad M, Subhash G, Loukus A (2004) Influence of end-conditions during tube hydroforming of aluminum extrusions. Int J Mech Sci 46:1195–1212
12. Nguyen TN, Wahab MA (1995) A theoretical study of the effect of weld geometry parameters on fatigue crack propagation life. Eng Fract Mech 51:1–18
13. Meinders T, van den Berg A, Huetink J (2000) Deep drawing simulations of tailored blanks and experimental verification. J Mater Process Technol 103:65–73
14. Zhao KM, Chun BK, Lee JK (2001) Finite element analysis of tailor-welded blanks. Finite Elem Anal Des 37:117–130
15. Natal Jorge RM, Roque AP, Valente RAF, Parente MPL, Fernandes AA (2007) Study of hydroformed tailor-welded tubular parts with dissimilar thickness. J Mater Process Technol 184:363–371
16. Raymond SD, Wild PM, Bayley CJ (2004) On modeling of the weld line in finite element analyses of tailor-welded blank forming operations. J Mater Process Technol 147:28–37
17. Loukus A, Subhash G, Imaninejad M (2004) Mechanical properties and microstructural characterization of extrusion welds in AA6082-T4. J Mater Sci 39:6561–6569
18. Valente RAF, Jorge RMN, Roque AP, Parente MPL, Fernandes AA (2008) Simulation of dissimilar tailor-welded tubular hydroforming processes using EAS-based solid finite elements. Int J Adv Manuf Technol 37:670–689
19. Abdullah K, Wild PM, Jeswiet JJ, Ghasempoor A (2001) Tensile testing for weld deformation properties in similar gage tailor welded blanks using the rule of mixtures. J Mater Process Technol 112:91–97
20. Liu S, Chao YJ (2005) Determination of global mechanical response of friction stir welded plates using local constitutive properties. Model Simul Mater Sci Eng 13:1–15
21. Kim D, Lee W, Kim J, Kim C, Chung K (2010) Formability evaluation of friction stir welded 6111-T4 sheet with respect to joining material direction. Int J Mech Sci 52:612–625
22. Lee W, Chung KH, Kim D, Kim J, Kim C, Okamoto K, Wagoner RH, Chung K (2009) Experimental and numerical study on formability of friction stir welded TWB sheets based on hemispherical dome stretch tests. Int J Plast 25:1626–1654
23. Zhan M, Du HF, Liu J, Ren N, Yang H, Jiang HM, Diao KS, Chen XP (2010) A method for establishing the plastic constitutive relationship of the weld bead and heat-affected zone of welded tubes based on the rule of mixtures and a microhardness test. Mater Sci Eng A 527:2864–2874
24. Waddell W, Jackson S, Wallach ER (1998) The influence of the weld structure on the formability of laser welded tailored blanks. SAE, Paper No. 982396
25. Kridli GT, Friedman PA, Sherman AM (2000) Formability of aluminum tailor-welded blanks. SAE, Paper No. 2000-01-0772
26. Chan LC, Chan SM, Cheng CH, Lee TC (2005) Formability and weld zone analysis of tailor-welded blanks for various thickness ratios. J Eng Mater Technol 127:179–185
27. Kim SW, Song WJ, Kang BS, Kim J (2009) Bursting failure prediction in tube hydroforming using FLSD. Int J Adv Manuf Technol 41:311–322